Selectivity of Metal Binding and Metal-Induced Stability of *Escherichia coli* NikR†

Sheila C. Wang, Alistair V. Dias, Stephanie L. Bloom, and Deborah B. Zamble*

Department of Chemistry, University of Toronto, Toronto, Ontario, Canada M5S 3H6

Received March 26, 2004; Revised Manuscript Received May 21, 2004

ABSTRACT: NikR from *Escherichia coli* is a nickel-responsive transcription factor that regulates the expression of a nickel ion transporter. Metal analysis reveals that NikR can bind a variety of divalent transition metals, including Ni(II), Cu(II), Zn(II), Co(II), and Cd(II). The selectivity of metal binding to NikR was investigated by using electronic absorption spectroscopy and small-molecule competitors. The relative affinities, Mn(II) < Co(II) < Ni(II) < Cu(II) ≥ Zn(II), follow the Irving−Williams series of metal-complex stabilities. Similar metal affinities were measured for the isolated metal-binding domain of NikR. To determine if any of these metal ions confer a differential effect on NikR, the stability of the metal-bound complexes was examined. In both thermal and chemical denaturation experiments, nickel binding stabilizes the protein more than any of the other metals tested. Thermal denaturation experiments indicate that metal dissociation occurs after loss of secondary structure, but there was no evidence for metal binding to unfolded protein following reversible chemical denaturation. These experiments demonstrate that, although several different metals can bind to NikR, nickel exerts a selective allosteric effect. The implications of these experiments on the in vivo role of NikR as a nickel metalloregulator are discussed.

Nickel ions are required by numerous organisms because they are catalytic cofactors of key metabolic enzymes (*1*, *2*). However, as with many other essential elements, the reactivity of nickel ions can result in detrimental cellular consequences (*3*, *4*), so they must be handled with care. It has become clear that to maintain healthy amounts of any transition metal in the cell the transporters responsible for importing or exporting the ions must be precisely regulated, usually at the transcriptional level (*5*, *6*). Nickel homeostasis is no exception, and along with nickel-specific membrane transporters (*7*, *8*), several nickel-responsive transcription factors have been identified. These metalloregulators include the SrnQ/SrnR complex in *Streptomyces griseus* (*9*), NmtR from *Mycobacterium tuberculosis* (*10*), NrsR from *Synechocystis* sp. PCC 6803 (*11*), and NikR from *Escherichia coli* (*E. coli*)[1] and *Helicobacter pylori* (*12*−*14*). To be accurate and efficient regulators, these factors must be selective for nickel versus other bioavailable metal ions, but how metal discrimination is achieved is not understood.

The *E. coli* NikR is a repressor protein that binds to the operator sequence of the *nik* operon and inhibits expression of the Nik transporter in the presence of excess nickel (*12*, *13*, *15*). NikR can be divided into two functional domains. The N-terminus of NikR is a ribbon−helix−helix DNA-binding domain, and the C-terminus contains a high-affinity nickel-binding site (*16*, *17*). On its own, the DNA-binding domain forms a dimer and only weakly binds the DNA operator (*16*), whereas the whole protein is a tetramer composed of two DNA-binding dimers and nickel induces tighter binding to the *nik* DNA sequence (*17*, *18*). Crystallographic analysis of the C-domain of NikR revealed four nickel ions bound to the tetramer in bridging sites between the dimer pairs (*18*). Each nickel ion is ligated by a square-planar coordination sphere composed of one cysteine and two histidine ligands from one monomer and a third histidine from the other (*18*). This type of metal-binding geometry was also observed in an extended X-ray absorption fine structure (EXAFS) study of the whole protein, but analysis of the isolated C-domain suggested that the protein was in fact a mixture of at least two different conformations (*19*). Furthermore, in the presence of DNA, the thiolate coordination to the nickel was no longer detected and a six-coordinate site was observed (*19*).

The square-planar geometry of the nickel-binding site of NikR suggests that a mechanism for metal selectivity could involve an arrangement of metal ligands in the apoprotein that favors nickel binding. Selective metal binding plays a significant role in the response of metalloregulators such as the Cu^{+}-sensing CueR and Zn^{2+}-sensing ZntR proteins (*20*), and the iron- or manganese-responsive DtxR/MntR repressors (*21*). This binding selectivity is due to the properties of the protein metal-binding sites that control metal ion affinities such as coordination number, geometry, composition, and overall charge. In the case of NikR, however, the variability of the nickel-binding site in the EXAFS study and the lack

† This work was supported by NSERC (Canada).

* To whom correspondence should be addressed. Phone: (416) 978-3568. E-mail: dzamble@chem.utoronto.ca.

[1] Abbreviations: DTNB, 5,5′-dithiobis(2-nitrobenzoic acid); DTT, dithiothreitol; *E. coli*, *Escherichia coli*; EDDA, ethylenediaminediacetic acid; EDTA, ethylenediaminetetraacetic acid (disodium salt); EGTA, ethylene glycol bis(2-aminoethyl ether)-*N*,*N*,*N*′,*N*′-tetraacetic acid; EXAFS, extended X-ray absorption fine structure; GHCl, guanidine hydrochloride; HEPES, 4-(2-hydroxyethyl)-1-piperazineethanesulfonic acid; ICP-AES, inductively coupled plasma atomic emission spectroscopy; MBD, the metal-binding domain of NikR, residues 49−133; NTA, nitrilotriacetic acid; PAGE, polyacrylamide gel electrophoresis; PAR, 4-(2-pyridylazo)resorcinol; Tris, tris(hydroxymethyl)aminomethane.

10.1021/bi049405c CCC: $27.50
Published on Web 07/17/2004

of preorganized ligands in the apo crystal structure demonstrate that the metal-binding site is not rigid (*18*, *19*). An alternative possibility is that only nickel ions can induce the conformational change that is required for the DNA-binding response (*18*). In an example of such a mechanism, studies of homologous CzrA and NmtR repressors demonstrated that, although several metals could bind to the proteins, only those inducing the correct coordination number and geometry had an allosteric effect (*22*).

To investigate the mechanism of the metal selectivity of NikR, we examined metal binding by NikR and the isolated metal-binding domain (MBD). Although both NikR and the MBD bind nickel ions with very high affinity, the proteins also bind other transition metals tightly. However, in both thermal and chemical denaturation experiments Ni(II) binding to NikR or the MBD conferred greater stability than any of the other transition metals analyzed. These experiments suggest that nickel induces a distinct conformational change in NikR, and the implications for nickel-selective allosteric control of NikR are discussed.

EXPERIMENTAL PROCEDURES

Materials. An 8 M high-purity stock solution of guanidine hydrochloride (GHCl) was purchased from Pierce. Chelex-100 was purchased from BioRad. All other reagents were molecular biology grade from Sigma except where noted. The plasmid pNIK103 was generously donated by P. Chivers (Washington University School of Medicine, St. Louis, MO) (*13*). Metal salts were a minimum of 99.9% pure and purchased from Aldrich. The concentrations of metal stocks prepared from these salts were confirmed by inductively coupled plasma atomic emission spectroscopy (ICP-AES). Assays were performed either with these stocks or with atomic absorption standard solutions (Aldrich). Buffers for all metal assays were treated with Chelex-100 to minimize trace metal contamination. Water was deionized on a Milli-Q water system (Millipore), and the pH of all Tris buffers was adjusted with HCl. All data were fitted by using Kaleidagraph 3.0 except where otherwise noted.

Protein Expression and Purification. The *E. coli* NikR protein was expressed from plasmid pNIK103 transformed into BL21(DE3) or BL21(DE3)pLysS cells, and purified on a Ni−NTA column (Qiagen) as previously described (*13*). Following the initial chromatography step, the eluted protein was dialyzed against 10 mM HEPES (pH 7.6), 100 mM KCl, 1 mM EDTA, and 1 mM DTT and stored at 4 °C.

An additional anion exchange column was used to remove small amounts of impurities eluted from the Ni−NTA column. The protein solution was loaded onto a MonoQ HR10/10 FPLC column (Pharmacia) in 20 mM Tris, pH 7.5, and eluted with a linear NaCl gradient. NikR came off the column at approximately 370 mM NaCl. The fractions were analyzed by using 15% SDS−PAGE, pure protein was pooled and concentrated with a centrifugal filter (Millipore, 5 kDa cutoff), and the buffer was exchanged on a PD-10 desalting column (Pharmacia) to 10 mM HEPES, pH 7.6, 100 mM KCl. The molecular mass of expressed NikR was verified by MALDI mass spectrometry (Hospital for Sick Children, Toronto). The observed mass was 15093.06 and 15096.59 Da on two different occasions, as compared to a calculated mass of 15093.7 Da. Protein concentrations in monomer equivalents were determined in 6 M GHCl by using an extinction coefficient at 276 nm of 4495 M^{-1} cm^{-1} (*23*).

To express residues 49−133 of NikR, which make up the metal-binding domain (MBD) (*17*), the gene sequence was PCR-amplified from pNIK103 by using the primers 5′-CACCCAGCATATGGGCACGCAAGGTTTCGCG and 5′-GTGGTGCTCGAGTCAATCTTCCTTCGGCAAGC and cloned into the *Nde*I and *Xho*I sites of pET24b (Novagen). The plasmid was sequenced (ACGT, Toronto), and the protein was expressed in *E coli* strain BL21(DE3). The MBD was purified with Ni−NTA and MonoQ chromatography as described for the whole protein except that the protein eluted from the MonoQ at approximately 250 mM NaCl. The molecular mass of the MBD was verified by ESI-MS, which revealed a mixture of peptides with and without the N-terminal methionine (calculated molecular mass 9699.8 Da, observed molecular mass 9699.5 and 9568.3 Da). The protein concentration was determined in 6 M GHCl by using the calculated extinction coefficient of 2680 M^{-1} cm^{-1} at 280 nm (*23*).

For experiments with either the whole protein or the MBD, only protein that was >90% reduced was used. If a higher level of oxidation was detected in the assay with 5,5′-dithiobis(2-nitrobenzoic acid) (DTNB; see below), protein samples were treated with 2 mM TCEP or 2 mM DTT for 12 h at 4 °C. The reducing agent was then removed by passing the protein twice over a PD-10 desalting column equilibrated in 10 mM HEPES, pH 7.6, 100 mM KCl.

DTNB Assay. Reactions contained 6 M GHCl, 0.3 mM DTNB, and a constant amount of protein buffer. The reactions were prepared at room temperature, and the absorbance was measured at 412 nm. A standard curve of β-mercaptoethanol solutions (final concentrations of 7−56 μM) was freshly prepared for each assay. NikR contains two cysteine residues. All of the subsequent experiments with the full protein were performed under aerobic conditions, and the oxidation state of the two cysteines of NikR or the MBD was monitored by DTNB assay. The protein was found to be stable in the presence of Ni(II) or Cu(II), with undetectable oxidation after incubation with the metals for 30 min, and less than 15% oxidation over a period of 48 h (data not shown).

Metal Analysis. One equivalent of metal ion was incubated with 17−25 μM NikR in 10 mM HEPES, pH 7.6, 100 mM KCl. After a 30 min incubation at 4 °C, unbound metal was removed on a PD-10 desalting column equilibrated with the same HEPES/KCl buffer, and the samples were analyzed by ICP-AES on an Optima 3000DV (Perkin-Elmer) equipped with a cross-flow nebulizer. Protein precipitation was observed with Zn(II), Cd(II), or Co(II), so 20 μM NTA was added with the metal in an effort to minimize aggregation. MBD samples were prepared by incubating the protein with 1.1 equiv of Ni(II), Cu(II), or Zn(II) overnight. In the case of Co(II), the protein was incubated with 2.1 equiv as 2:1 binding was initially suspected. After the incubation period the samples were dialyzed against chelexed buffer (10 mM HEPES, pH 7.6, 100 mM KCl) to remove unbound metal.

UV−Vis Spectroscopy and Competition Assays. Electronic absorption spectra were collected at 25 °C on an Agilent 8453 spectrophotometer equipped with an 89090A Peltier

Table 1: Metal Binding to NikR

metal	% metal[a]	K_{Me} (M)	λ_{max} (nm) (ϵ_c, $M^{-1}\,cm^{-1}$)
Co(II)	51 ± 16 (2)[b]	$(2 \pm 1) \times 10^{-9}$ [d]	307 (1100)
Ni(II)	96 ± 5 (4)	$(9.3 \pm 0.7) \times 10^{-13}$ (0.94 ± 0.05)[e]	302 (7200)
Cu(II)	80 ± 14 (3)	$(1.4 \pm 0.3) \times 10^{-17}$ (0.9 ± 0.2)[e]	388 (4450)
Zn(II)	83 ± 18 (2)[b]	$<1 \times 10^{-12}$ [f]	
Cd(II)	n/d[b,c]	$<1 \times 10^{-9}$ [f]	
Mn(II)	0.02 ± 0.01 (3)	n/d	

[a] The protein was incubated with stoichiometric amounts of metal followed by gel filtration chromatography and protein quantitation. The percent metal ± standard deviation as determined by ICP-AES analysis is reported, and the number of trials performed is indicated in parentheses. [b] NikR was incubated with stoichiometric amounts of metal in the presence of NTA. All of the protein in the presence of Cd(II) precipitated prior to gel filtration. [c] Not determined. [d] Estimated from competition experiments with Fura2. [e] The data were fitted to a Hill binding equation as described in the Experimental Procedures. K_{Me} represents the free metal concentration at half-maximal binding, the errors listed are the standard deviations, and the Hill coefficients are listed in parentheses. [f] Estimated from competition experiments with PAR.

temperature controller. All experiments contained 20−100 μM NikR, 10 mM HEPES, pH 7.6, 100 mM KCl, and metal and competitor concentrations as noted. Titration experiments with NikR (but not the MBD) contained 20 mM glycine to minimize precipitation, and in most cases they were performed with a separate aliquot of protein for each concentration of metal. The samples were incubated at room temperature for a minimum of 1 h and typically overnight. If experiments were performed with multiple additions of metal to a single aliquot, the baseline of the UV spectrum was monitored at 500 or 700 nm, depending on the metal, to ensure that the protein was not aggregated before the subsequent metal addition. The extinction coefficients of the protein−metal complexes (Table 1) were determined by plotting the absorbance versus metal concentration and fitting the data to a straight line. The fraction of metal-bound protein in the competition experiments was calculated by using these extinction coefficients. For the cobalt complexes of the whole protein, because precipitation precluded saturation, the extinction coefficient was confirmed by determining the absorption spectrum after removal of unbound metal on a PD-10 column and measuring the bound metal concentration with a 4-(2-pyridylazo)resorcinol (PAR) assay (see below).

The metal-affinity constants of the competitors were obtained from the National Institute of Science and Technology (NIST) database of critically selected stability constants of metal complexes, version 7.0 (*24*), as were the protonation constants for the chelators and metal-bound chelators, and protonation constants of aqueous metal ions were obtained from Perrin and Boyd (*25*). The apparent constants at a pH of 7.6 and an ionic strength of 0.1 were then calculated by using the equations described by Fahrni et al. (*26*), resulting in a $K_{d(app)}$ of 5.21×10^{-11}, 1.31×10^{-14}, and 4.75×10^{-15} M for Ni(II)−EGTA, Cu(II)−EDDA, and Cu(II)−EGTA complexes, respectively. These constants were used to solve the quadratic equation

$$([Me]_T - [MeNikR])[C]_T - [MeC]([C]_T + [Me]_T - [MeNikR] + K_{d(app)}) + [MeC]^2 = 0$$

where $[Me]_T$ is the total concentration of metal used, $[C]_T$ is the total concentration of competitor used, and [MeC] and [MeNikR] indicate the concentrations of metal−competitor and metal−protein complexes. This equation was solved for [MeC], and the free metal concentration was calculated by subtracting [MeC] and [MeNikR] from $[Me]_T$. The data were fitted to a Langmuir equation with a variable Hill coefficient n: $r = [Me]^n/((K_{d(app)})^n + [Me]^n)$, where r is the fraction of protein bound to metal and $K_{d(app)}$ represents the free metal concentration required for 50% binding.

PAR Competition Experiments. Increasing amounts of MBD were added to aliquots of 300 μM PAR (Sigma) containing 10 μM Zn(II) or 8 μM Cd(II) in 10 mM HEPES, pH 7.6, 100 mM KCl. The samples were equilibrated for 20 min at room temperature, and then the absorption at 500 and 510 nm was measured for the Zn(II) and Cd(II) experiments, respectively. Titration of PAR with metal atomic absorption standards under the same conditions was used to measure extinction coefficients of 52300 M^{-1} cm^{-1} at 500 nm for Zn(II) and 21400 M^{-1} cm^{-1} at 510 nm for Cd(II).

Fura-2 Competition Experiments. Increasing amounts of NikR or the MBD were added to separate aliquots containing 50 μM Fura-2 (Molecular Probes) previously incubated with 10 or 15 μM Co(II) atomic absorption standards for 1 h in the dark at room temperature. Following protein addition, the reactions were left to equilibrate for 24 h in the dark at room temperature and subsequently monitored by UV−vis spectroscopy at 368 nm. An extinction coefficient of −20500 M^{-1} cm^{-1} at 368 nm was measured by titration of Fura-2 with the Co(II) atomic absorption standards under the same conditions. The amount of free Co(II) was estimated by using $K_D = 8.64$ nM for the Co(II)−Fura2 complex (*27*), and then the K_D for Co(II)−NikR was calculated from $[Co(II)]_{free}$, $[Co(II)-NikR] = [Co(II)]_T - [Co(II)]_{free} - [Co(II)-Fura2]$, and $[NikR]_{free} = [NikR]_T - [Co(II)-NikR]$.

Measurement of Protein Stability. Thermal denaturation was monitored by circular dichroism on a Jasco model J-810 spectropolarimeter in a cell with a 0.1 cm optical path length over a temperature range of 4−110 °C. The temperatures were controlled by a Peltier device. Scan speeds of 2 °C/min and 1 min/nm with a spectral bandwidth of 1.0 nm were used. The experiments were performed by using protein stocks dialyzed against filtered 25 mM potassium phosphate, pH 7.6, at concentrations ranging from 5 to 20 μM. Thermal denaturation was monitored by changes in θ (mdeg) at 222 nm. The spectrum of each sample was corrected by subtraction of the buffer alone.

Thermal denaturation was also monitored by electronic absorption spectroscopy on the instrument described above. UV−vis spectra were collected every 2 °C after equilibration for 1 min.

GHCl denaturation was monitored by circular dichroism on a Jasco model J-710 spectropolarimeter in a cylindrical

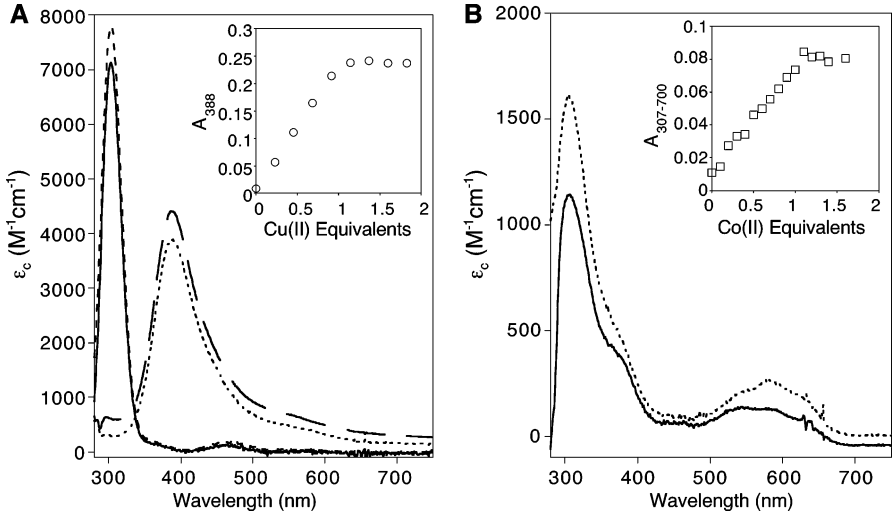

FIGURE 1: Metal binding to NikR and the MBD of NikR. (A) The spectra of Ni(II) bound to NikR (solid line) or the MBD (dashed line) and Cu(II) bound to NikR (large dashes) or the MBD (small dashes) were generated by subtracting the spectra of the apoproteins from the spectra of the metal-saturated proteins. Inset: Titration of 53 μM NikR with $CuSO_4$ produces a linear increase in the absorbance at 388 nm with a slope of 4450 M^{-1} cm^{-1} that saturates at stoichiometric metal ions per protein monomers. (B) The spectrum of Co(II)-substituted NikR (solid line) was generated by subtracting the spectrum of the apoprotein from that of NikR titrated with 0.4 equiv of $CoSO_4$. The spectrum of Co(II)-substituted MBD (dashed line) was generated by subtracting that of apoprotein from that of Co(II)-saturated protein. Inset: Titration of 40 μM of the MBD with Co(II) produces a linear increase in the absorbance at 307 nm with a slope of 1600 M^{-1} cm^{-1} that saturates at 1.1 equiv of cobalt per protein monomer. The difference of absorbance between 307 and 700 nm is shown to account for precipitation after stoichiometric amounts of metal were added.

cell of 0.1 cm optical path length over a wavelength range from 260 to 195 nm at room temperature. Each CD spectrum was the average of five accumulations at a scanning speed of 50 nm/min, a 1.0 nm spectral bandwidth, a data pitch of 0.1 nm, and a 4 s response time. The experiments were performed by using protein stocks dialyzed against 10 mM HEPES, 100 mM KCl, pH 7.6, at concentrations ranging from 5 to 40 μM. For experiments performed in the presence of metal, the protein was incubated overnight with stoichiometric amounts of metal sulfate. The concentrations of the holoprotein stocks were verified by UV−vis spectrophotometry in 6 M GHCl. The protein was incubated overnight at each GHCl concentration. Prior to CD measurements being taken, the samples were centrifuged to remove precipitate. Denaturation was monitored by changes in θ (mdeg) at 222 nm. The spectrum of each sample was corrected by subtraction of the buffer alone.

All denaturation data were fitted to a sigmoidal Boltzmann curve by using Origin 5.0. The minimum and maximum ellipticities (θ) were used to calculate the fractional change in ellipticity (FCE) at 222 nm by using the equation $(\theta_{folded} - \theta_{obs})/(\theta_{folded} - \theta_{unfolded})$ (*28*). The T_M and G_M values are the temperatures and GHCl concentrations, respectively, required to reach 50% denaturation of the protein.

The data for GHCl denaturation of full-length NikR and MBD could not be fitted to a variety of equilibrium models including dimer-unfolded monomer, tetramer-unfolded monomer, and tetramer−dimer-unfolded monomer (*28*).

Attempts were also made to fit the data to a two-state linear denaturant binding model involving only folded and unfolded states, or a three-state model which incorporates a third, intermediate species in the unfolding mechanism (*29*, *30*). The calculated values for the equilibrium constant (K^{H_2O}) varied drastically between different trials, so again, the data could not be fitted to these models.

RESULTS

Metal Binding to NikR. Previous spectroscopic and structural studies demonstrated that NikR binds nickel ions in stoichiometric amounts (*13*, *18*, *19*). In this study metal analysis and electronic absorption spectroscopy were used to investigate the metal-binding selectivity of NikR. The metal-binding activities of both the whole protein and the isolated C-terminal MBD were examined. The ligands of the high-affinity metal-binding site of NikR are located in the C-terminal domain of the protein (*18*), and like the whole protein, the apo-MBD (residues 49−133) at micromolar concentrations forms a tetramer (*17*, *18*). Furthermore, the MBD folds into a stable metal-binding peptide with an overall structure and nickel affinity similar to those of the whole protein (*17*, *18*), indicating that the high-affinity metal-binding site is preserved in this construct.

To determine if NikR can bind divalent transition metals other than nickel, the protein was incubated with stoichiometric amounts of metal, followed by gel filtration chromatography to remove any unbound or weakly bound ions. ICP-AES confirmed that NikR binds stoichiometric nickel and revealed stoichiometric copper or zinc bound (Table 1). Precipitation resulted in only substoichiometric cobalt, and prevented analysis of the Cd(II)-treated protein or protein treated with more than 1 equiv of metal, so it was not possible to use ICP-AES to determine if NikR can bind more than 1:1 metal (data not shown). Binding by manganese was too weak to be detected in this experiment.

The absorption spectra of Ni(II), Cu(II), or Co(II) bound to NikR or the MBD are shown in Figure 1, and the calculated extinction coefficients are listed in Tables 1 and 2. Saturation was observed with 1:1 nickel as previously reported (ref *13* and data not shown) and 1:1 copper (Figure 1A). The features of the nickel spectra, including a single absorption band between 400 and 550 nm (ϵ_c = 125 M^{-1} cm^{-1}) with no appreciable absorption at lower energy, are

Table 2: Metal Binding to MBD

metal	K_{Me} (M)	λ_{max} (nm) (ϵ_c, $M^{-1}cm^{-1}$)
Co(II)	$(4 \pm 2) \times 10^{-9}$ [a]	307 (1600)
Ni(II)	$(3 \pm 1) \times 10^{-12}$ (0.7 ± 0.2)[b]	302 (7600)
Cu(II)	$(2.1 \pm 0.8) \times 10^{-17}$ (0.9 ± 0.2)[b]	388 (3900)
Zn(II)	$<1 \times 10^{-12}$ [c]	
Cd(II)	$<1 \times 10^{-9}$ [c]	

[a] Estimated from competition experiments with Fura2. [b] The data were fitted to a Hill binding equation as described in the Experimental Procedures. K_{Me} represents the free metal concentration at half-maximal binding, the errors listed are the standard deviations, and the Hill coefficients are listed in parentheses. [c] Estimated from competition experiments with PAR.

similar to those of nickel-substituted mutant zinc-finger peptides (*31*), and are characteristic of four-coordinate nickel ligated in a square-planar or distorted square-planar geometry (*31*, *32*). The difference spectrum of Cu(II) bound to NikR has an intense broad band with a maximum absorption at 388 nm, and a poorly defined lower energy band centered around 550 nm. This spectrum is also suggestive of a square-planar or distorted square-planar geometry with at least one thiolate ligand (*32*−*35*), but additional spectroscopy will be necessary to confirm this geometry (*32*).

Saturation at 1:1 metal ion per protein was also observed upon titration of the MBD with Co(II) (Figure 1B inset), but the spectrum of the Co(II)-bound MBD is slightly different from that of the whole protein (Figure 1B). The electronic absorption spectra of cobalt-substituted proteins have been studied in detail (*36*, *37*). For the whole protein spectrum, both tetrahedral and octahedral geometries can be excluded on the basis of the intensities of the d−d transition bands (60−80 M^{-1} cm^{-1}); however, it is not possible to differentiate among square-planar, square-pyramidal or tetragonal coordination geometries, which have very similar spectra (*32*). The estimated extinction coefficient of 1100 M^{-1} cm^{-1} at 307 nm is indicative of Co(II)−thiolate charge transfer from a single cysteine ligand on the basis of a comparison with proteins and model complexes that exhibit intensities of 900−1300 M^{-1} cm^{-1} per Co(II)−thiolate (refs *38* and *39* and references therein). The 307 nm band of Co(II)−MBD has an extinction coefficient of 1600 M^{-1} cm^{-1}, almost 50% larger than that observed with the whole protein, and the extinction coefficient at 580 nm has also increased to 250 M^{-1} cm^{-1}.

Metal-Binding Affinity to NikR. The affinity of NikR for all of the metals with stoichiometric binding was too high to measure by direct titration. To measure the affinity of NikR or the MBD for nickel or copper, metal-buffered systems similar to that described for several zinc complexes were used (*26*, *40*). Titration of NikR with nickel in the presence of EGTA (Figure 2A) revealed that NikR binds stoichiometric nickel with picomolar affinity (K_{Me1} = $(9.4 \pm 0.2) \times 10^{-13}$ M). While this work was in progress, a similar nickel affinity of 7 pM was reported (*17*). Copper-buffered titrations were performed in the presence of either EGTA or EDDA (Figure 2A), and a fit of the compiled data revealed a $K_{Me1} = (8.4 \pm 0.3) \times 10^{-18}$ M. The binding constants of the MBD for Ni(II) or Cu(II) were consistent with those determined for the whole protein, although slightly weaker (Table 2).

To determine the affinity of NikR for zinc ions, a competition assay was performed with the colorimetric indicator PAR, which binds Zn(II) in a 2:1 complex with a strong absorbance at 500 nm (*41*, *42*). Competition experiments revealed that both NikR and the MBD bind Zn(II) tighter than PAR (Figure 2B and data not shown), but complete metal titrations were possible only with the MBD. The affinity of PAR for zinc is pH dependent (*41*, *42*), and at pH 7.6 PAR is expected to form 1:1 and 2:1 zinc complexes with stepwise affinity constants of 1.2×10^7 and 6.7×10^5 M^{-1}, producing an overall stability constant of 8.1×10^{12} M^{-2}. An estimation of the concentration of Zn(II)−MBD by using methods previously described (*43*) indicates that the protein quantitatively removes Zn(II) from the Zn(II)−$(PAR)_2$ complex. If all of the zinc not bound to PAR is bound by NikR, then a conservative upper limit of 10^{-12} M can be estimated for the binding of Zn(II) to NikR or the MBD.

Similar competition experiments with Cd(II) suggested that NikR (data not shown) and the MBD (Figure 2B) also bind

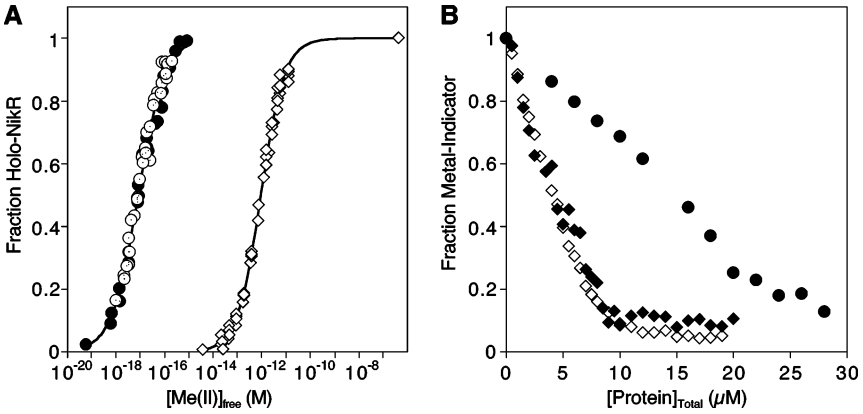

FIGURE 2: Metal affinity of NikR and the MBD. (A) Titration of NikR with $NiSO_4$ in the presence of EGTA (tilted squares) or with $CuSO_4$ in the presence of EGTA (open circles) or EDDA (filled circles). The data were fitted to a Hill curve as described in the Experimental Procedures, and the calculated K_{Me} values are listed in Table 1. (B) Titration of 300 μM PAR and 10 μM Zn(II) with the MBD of NikR (open tilted squares), 300 μM PAR and 8 μM Cd(II) with the MBD (closed tilted squares), or 50 μM Fura2 and 10 μM Co(II) with NikR (closed circles). The decrease in the fraction of the appropriate metal−indicator complex with protein addition was monitored at 500 nm for Zn(II)−$(PAR)_2$, 510 nm for Cd(II)−$(PAR)_2$, and 368 nm for Co(II)−Fura2. At more than 20 μM NikR less than 5% Fura2 was in a complex with Co(II), and the changes in absorbance measurements were <0.05, so some variability in the data was observed. All experiments were performed in 10 mM HEPES, pH 7.6, 100 mM KCl.

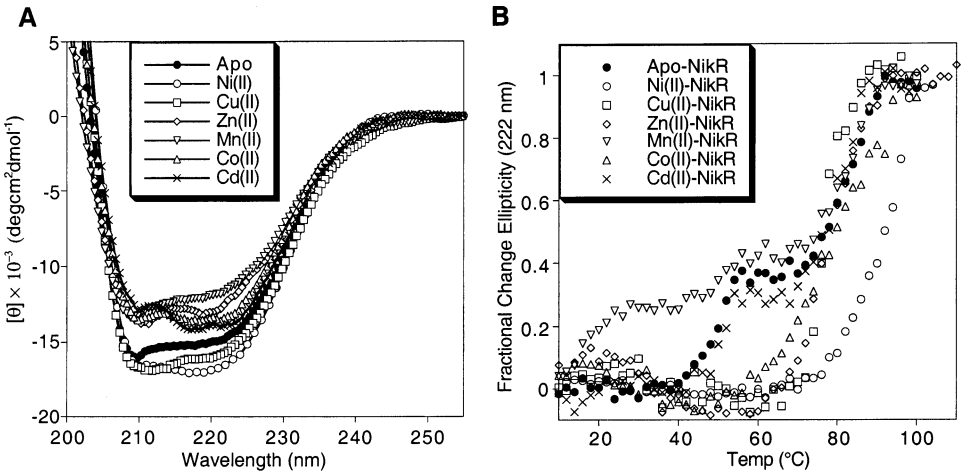

FIGURE 3: Effect of Me(II) on NikR secondary structure and stability. (A) Far-UV CD spectra of apo-NikR and NikR incubated with stoichiometric amounts of the indicated divalent transition metals. Only every fifth data point is shown for clarity. (B) Thermal denaturation of 5 μM NikR in the presence or absence of 1 equiv of the metals indicated. The CD spectra were monitored at 222 nm, and the fractional change in ellipticity was calculated as described in the Experimental Procedures. Data were obtained in 25 mM potassium phosphate, pH 7.6.

Cd(II) more tightly than PAR. Stepwise affinity constants of 1.0×10^5 and 7.1×10^4 M^{-1} can be estimated from literature values (*41*, *44*; the Cd(II) studies were performed at zero ionic strength), and an upper limit of Cd(II) binding to NikR is estimated at 10^{-9} M. Direct titration of NikR or the MBD with Cd(II) did not produce a detectable change in the UV−vis spectrum (data not shown). Thiolate−Cd(II) bonds have strong ligand-to-metal charge-transfer bands at 240−250 nm with estimated extinction coefficients of 6000−6500 cm^{-1} M^{-1} (*45*, *46*). Although Cd(II) can induce DNA binding (*47*), the lack of such a band in the NikR−Cd(II) complex suggests that Cd(II) is bound in a coordination sphere with a different composition than that of Ni(II).

To estimate the binding affinity of NikR for Co(II), competition experiments with the fluorescence indicator Fura-2 were performed. The Co(II)−Fura2 complex has a K_D of 8.64×10^{-9} M at pH 7 (*27*), and because the affinity of Fura-2 for metals is not affected around neutral pH (*48*), we used this number for our calculations. NikR was titrated into solutions of 50 and 10−15 μM Co(II) (Figure 2B). Only numbers from data with more than 5% Fura2 in a complex with Co(II) were used, because the error in the measurements at lower amounts of Co(II)−Fura2 was quite large. Data from more than 20 measurements were used to estimate a K_D of $(2 \pm 1) \times 10^{-9}$ M for the Co(II)−NikR complex. Similar experiments with the MBD were used to estimate a K_D of $(4 \pm 2) \times 10^{-9}$ M.

Protein precipitation prevented any spectroscopic competition experiments with two different metals. In an effort to compare the coordination by the different metals we examined the thiol reactivity of the metal-bound complexes. The nickel site includes coordination to Cys95 (*18*, *19*), and only one of the two cysteines of NikR is detected in the Ni(II) complex, presumably because nickel coordination to Cys95 is strong enough to block the reaction with DTNB (ref *19* and data not shown). Similarly, Cu(II) binding to NikR results in only one detectable free thiol. Neither zinc nor cobalt blocks the DTNB reaction with the two cysteines (data not shown) even though the Co(II)−NikR spectrum indicates thiolate coordination, suggesting either that the metal binding is too weak to block DTNB reactivity or that the site is fluctuating between two different conformations.

Stability of Holo-NikR. To investigate the effects of the different divalent metals on the secondary structure and protein stability of NikR CD experiments were performed. Stoichiometric nickel induces a small increase in secondary structure (*17*). Other divalent metals also induce small changes in the overall secondary structure (Figure 3A), with Cu(II)−NikR having the spectrum most similar to that of Ni(II)−NikR.

A previous report on urea denaturation experiments demonstrated that NikR denatures in two distinct phases that correspond to the separate melting of the DNA-binding and metal-binding domains (*17*). Similarly, thermal denaturation of apo-NikR occurs over two phases (Figure 3B); the first phase of thermal denaturation occurs over a T_M of 50 °C, close to the 46 °C T_M of apo-MBD (Table 3), and the second denaturation occurs at 84 °C. In the presence of 1 equiv of nickel, both NikR and the MBD are stabilized such that there is only one denaturation step at 98 and 94 °C, respectively (Figure 3B and data not shown). None of the other metals investigated stabilize the protein as much as nickel, although a smaller degree of stabilization was observed with Cu(II), Zn(II), and Co(II). In each case the T_M values of the whole protein were similar to those of the MBD (Table 3). Denaturation in these experiments was not reversible, so it is not possible to calculate thermodynamic values, but they do provide qualitative information about the stability of the protein bound to different metal ions (*49*).

Many cofactor-containing proteins unfold through an intermediate in which the cofactor is bound to unfolded protein (*50*−*53*). To determine if nickel was still bound to NikR after thermal denaturation, the absorption spectrum was monitored. Under the same heating conditions used in the CD experiments, the nickel signal at 302 nm was still apparent above 94 °C, the T_M of the protein (Figure 4A), although at very high temperatures some evidence for protein aggregation was observed (Figure 4A). The similarities in the electronic absorption spectra of the nickel-bound native and denatured proteins suggest that the metal is bound in the same type of environment in both states of the protein (data not shown). If the protein was held at 100 °C, then the nickel signal eventually disappeared over about 20−30 min (data not shown). In a similar experiment, there was no

Table 3: Metal Stabilization of NikR and the MBD

metal	NikR T_M[a,b] (°C)	MBD T_M[a] (°C)	metal	NikR T_M[a,b] (°C)	MBD T_M[a] (°C)
apo	49.7 ± 0.8, 84 ± 2 (6)	46 ± 2 (4)	Mn(II)	16 ± 2, 50 ± 1, 82 ± 2 (2)	n/d[c]
Ni(II)	98 ± 1 (5)	94 ± 1 (4)	Co(II)	78 ± 3 (4)	64.5 ± 0.7 (2)
Cu(II)	77 ± 1 (5)	77.5 ± 0.7 (2)	Cd(II)	51 ± 1, 80 ± 2 (2)	57 ± 2 (2)
Zn(II)	78.5 ± 0.7 (3)	71.5 ± 0.7 (2)			

[a] T_M is the temperature at which the protein is half-denatured and is calculated by fitting the data to a Boltzmann sigmoidal curve by using Origin 5.0. Errors listed are standard deviations, and the number of experiments performed is indicated in parentheses. [b] If two denaturation phases were observed, each phase was fitted separately, and the melting temperatures are listed. Three phases were observed with Mn(II)−NikR. [c] Not determined.

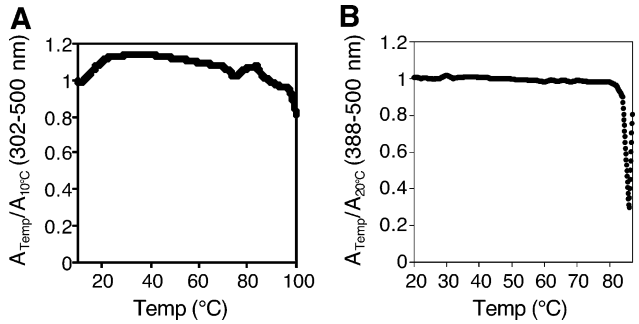

FIGURE 4: Metal dissociation upon thermal denaturation of NikR. The electronic absorption spectra of 20 μM NikR bound to Ni(II) (A) or Cu(II) (B) were monitored. The fraction of the signal remaining at each temperature at 302 nm (A) or 388 nm (B) was plotted. The spectra were obtained every 2 °C, and the rate of temperature change was the same as that used in the CD experiments shown in Figure 3. The absorbance at 500 nm was subtracted to minimize any apparent effects of precipitation, but by 88 °C in the Cu(II) melt all of the protein had precipitated. Data were obtained in 10 mM HEPES, 100 mM KCl, pH 7.6.

evidence for the loss of copper binding until the protein was heated past 80 °C (Figure 4B), above the T_M of 77 °C for melting of the secondary structure. Both of these experiments indicate that unfolded protein still binds a metal ion that is lost over time.

The relative stabilization conferred by divalent metals on NikR and the MBD in the thermal melts was confirmed by chemical denaturation experiments in GHCl. In these experiments, the protein samples were allowed to reach equilibrium by incubating overnight. Again, the denaturation of apo-NikR occurs over two phases, at 1.2 and 2.8 M GHCl (Figure 5A), whereas Ni(II)−NikR denatures in one phase at 3.4 M GHCl as does Ni(II)−MBD (Figure 5B). Nickel holds the secondary structure of NikR and the MBD intact at higher concentrations of denaturant than any of the other metals (Table 4 and Figure 5). The same samples were also examined with absorption spectroscopy, which demonstrated that metal dissociation coincides with loss of secondary structure (data not shown). To determine if the denaturation proceeded through a metal-bound unfolded intermediate, the denaturation was monitored over time by using both the CD and the UV spectrophotometer. Although the apoprotein denatured within minutes, the nickel-bound proteins denatured over a course of several hours, and the loss of secondary structure and metal dissociation was concerted (data not shown).

In contrast to the thermal experiments, denaturation of apo-NikR or Ni(II)−NikR with GHCl was reversible (data not shown and Figure 6). The addition of nickel to unfolded apo-NikR in 2.5 M GHCl resulted in almost a complete restoration of secondary structure and the same absorption spectrum as that observed for Ni(II)−NikR. At 3 M GHCl the holoprotein is partially unfolded, so only a fraction of metal binding and refolding is restored, and at 4 M GHCl, the protein remained denatured and nickel binding was not detected. More than stoichiometric amounts of Ni(II) did not improve the folding, providing further evidence that NikR is not denaturing through a metal-bound intermediate.

DISCUSSION

The square-planar geometry of the nickel coordination sphere of NikR suggested by the solution spectrum of

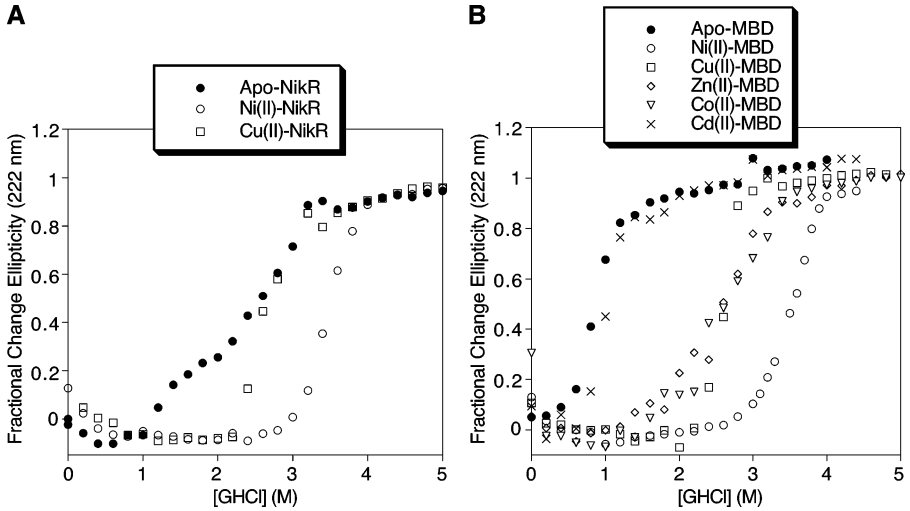

FIGURE 5: Chemical denaturation of NikR and the MBD. Aliquots of 20 μM NikR (A) or 40 μM MBD (B) and stoichiometric amounts of divalent metals were incubated overnight with increasing concentrations of GHCl at room temperature. The CD spectra were obtained, and the fractional change in ellipticity was calculated as described in the Experimental Procedures. The data were obtained in 10 mM HEPES, pH 7.6, 100 mM KCl.

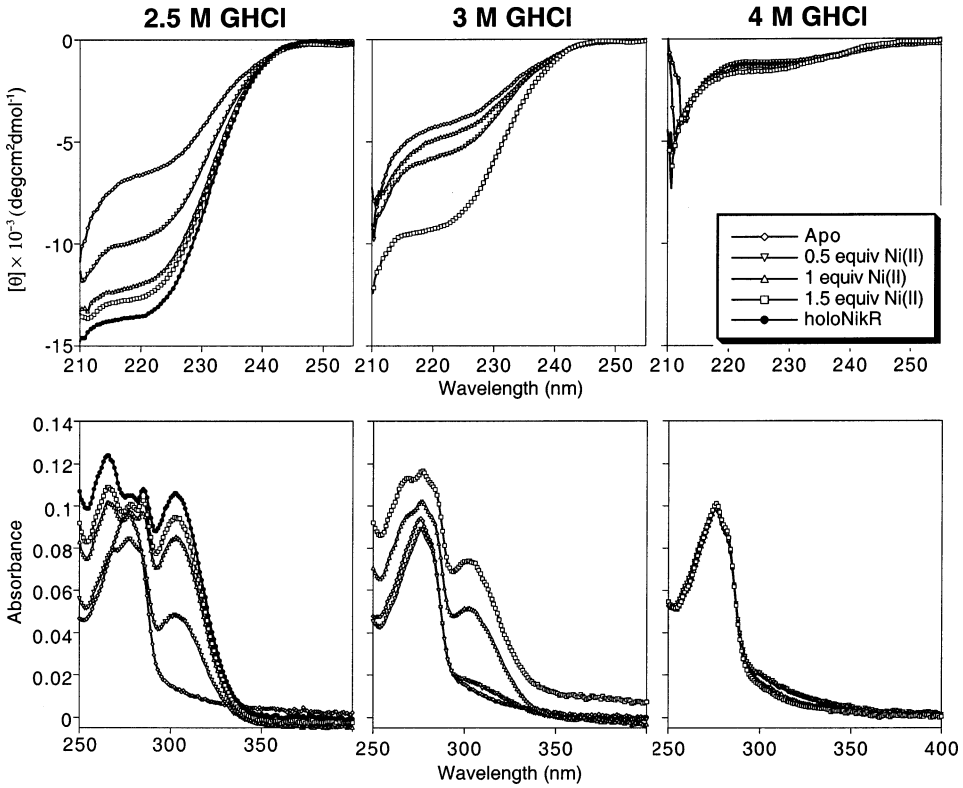

FIGURE 6: Renaturation of Ni(II)−NikR. Apo-NikR (20 μM in 10 mM HEPES, 100 mM KCl, pH 7.6) was preincubated for 5 min in 2.5, 3, or 4 M GHCl followed by the addition of the indicated amounts of Ni(II). The samples were then left to equilibrate overnight at room temperature before the CD (top, every fifth data point shown for clarity) and electronic absorption spectra (bottom) were obtained. Ni(II)−NikR was also incubated overnight in 2.5 M GHCl, and the spectra are shown.

Ni(II)−NikR is in agreement with both the EXAFS analysis of holo-NikR and the high-resolution structural analysis of the C-terminal domain (*18*, *19*). This type of geometry is favorable for four-coordinate Ni(II) (*54*), so it is reasonable to suggest that the protein could have metal-selective binding activity. However, NikR not only binds nickel with high picomolar affinity but also tightly binds several other metal ions such as Cu(II), Zn(II), Co(II), and Cd(II). The fact that stoichiometric amounts of all of these metals induce DNA binding (*47*) suggests that they bind to the same place on NikR. Furthermore, competition experiments in the context of the DNA-binding activity induced by the different metals indicate that copper replaces nickel in equilibrium conditions (*47*).

Small-molecule complexes with square-planar geometry have been reported for all of the metal ions that bind to NikR, but with the exception of Cu(II) complexes they are not very common (*54*, *55*), and this type of geometry is rarely if at all observed in protein complexes (*55*). The electronic absorption spectra of Cu(II)− and Co(II)−NikR are suggestive of square-planar coordination, but other geometries cannot be ruled out. Furthermore, a thiolate ligand is not indicated by the Cd(II) spectra, the protein can bind zinc with high affinity, but the ion does not block the reactivity of the cysteine thiolate with DTNB, and the Co(II) spectra of the NikR and MBD complexes are not the same. These observations are consistent with the flexible coordination at the binding site demonstrated by the EXAFS analysis (*19*).

Thus, it is likely that NikR accommodates metals in an adaptable manner such that it is able to bind a variety of divalent metals with very high affinity. This hypothesis is supported by the relative affinities of the first-row divalent transition metals, $Mn^{2+} < Co^{2+} < Ni^{2+} < Cu^{2+} \geq Zn^{2+}$, which mirrors the Irving−Williams series (*56*). This series is the general trend in metal ion affinities observed for small-molecule chelators. The observation that metal binding to NikR follows the same trend suggests that it is the inherent properties of the metal ions that dictate the strength of the metal−protein complex, not a particular property of NikR. A similar observation was made in a recent study of human carbonic anhydrase II, which also demonstrated a metal ion selectivity that follows the Irving−Williams series except with mutants that changed and constrained the coordination number or geometry of the metal-binding site (*57*).

Picomolar or higher metal affinities have been reported for other metalloregulatory proteins (*5*, *6*). As with these other systems, the extremely tight nickel binding by NikR means that the apoprotein binds metal ions at a concentration lower than that of one "free" nickel ion in the cell. This threshold raises the question of how proteins that have a functional use for nickel could compete with NikR and acquire nickel before the import pathway is shut down. One possible explanation is that the high-affinity site on NikR is not the sole control point of nickel homeostasis, a hypothesis supported by studies of the metal-induced DNA-binding activity of NikR (*17*, *47*). In the case of NikR, the issue is further complicated by the fact that it binds tightly to other types of physiological metals and thus could compete with metalloproteins outside the nickel pathways. There is no evidence to suggest that NikR interferes with other types of metal homeostasis or inappropriately responds to other metals. Clearly, the thermodynamics of metal binding are only one piece of the pathway, and as previously discussed, the kinetics of metal exchange may be important for

Table 4: Chemical Denaturation of NikR and the MBD

metal	NikR G_M[a], (M)	MBD G_M[a] (M)	metal	NikR G_M[a,b] (M)	MBD G_M[a] (M)
apo	1.2 ± 0.1, 2.8 ± 0.1 (4)	0.9 (1)	Zn(II)	n/d[c]	2.6 (1)
Ni(II)	3.4 ± 0.2 (4)	3.4 ± 0.1 (2)	Co(II)	n/d	2.7 (1)
Cu(II)	2.7 ± 0.2 (4)	2.6 (1)	Cd(II)	n/d	1.0 (1)

[a] G_M is the concentration of GHCl at which the protein is half-denatured and is calculated by fitting the data to a Boltzmann sigmoidal curve by using Origin 5.0. Errors listed are standard deviations, and the number of experiments performed is indicated in parentheses. [b] If two denaturation phases were observed, each phase was fitted separately, and the G_M values are listed. [c] Not determined.

metalloproteins to overcome the apparent thermodynamic barriers to metal accessibility (*5*, *6*).

The chemical denaturation experiments of NikR reveal that there is communication between the two domains. Denaturation of the Ni(II)-loaded protein was not detected much below 3 M GHCl, whereas denaturation of both domains of the apoprotein was complete at that concentration, indicating that nickel binding to NikR stabilizes both the metal-binding domain and the DNA-binding domain. This connection between the domains is not surprising given the allosteric control of nickel binding on the DNA-binding activity, and was also indicated in the EXAFS studies which demonstrated that DNA binding affects the metal-coordination sphere (*19*). This effect seems to be specific for nickel because none of the other metals examined induced a T_M or G_M higher than that of the DNA-binding domain in the apoprotein.

The apparent single-step denaturation of the holoproteins cannot be cleanly fitted to any simple denaturation model, likely because there are folding intermediates such as those postulated for all but very small proteins (*58*). Additional studies are needed to complete the thermodynamic analysis of NikR. However, the fact that nickel affords greater stability toward both thermal and chemical denaturation than other metal ions provides a qualitative indication of a differential effect of nickel on NikR that is not reflected by the relative metal-binding affinities. There are other examples of proteins in which the presence of the cofactor does not influence the structural stability as much as predicted from the energetics of cofactor binding. This discrepancy was explained by the observation that unfolded protein can reversibly bind the cofactor. For example, evidence for cofactor binding to unfolded protein in vitro was observed in studies of heme binding to cytochrome b562 (*51*), and noncovalent cofactor binding to denatured protein has been directly observed in several systems including an FMN-binding flavodoxin (*52*), and a zinc- or copper-loaded azurin (*50*). Nickel binding to unfolded NikR is observed in the thermal denaturation experiments described here, but the metal is lost over time, and the thermal denaturation of NikR is not reversible. Furthermore, under the equilibrium conditions of the chemical denaturation experiments metal binding to the unfolded NikR is not detected, so metal binding to a denatured intermediate cannot be invoked to explain the lack of correlation with metal-binding affinities.

In many other studies, an increase in cofactor affinity translates into increased stability (for example, see refs *50* and *59*), as one would expect for a simple thermodynamic cycle involving apo, holo, and unfolded states. However, in these cases the cofactors were permanent components of the active protein such that the activity of these proteins did not involve a cofactor-binding step. The function of NikR must be controlled by an active response to the metal ion, and in that respect it more closely resembles an enzyme responding to substrate. Just as an enzyme can harness the binding energy of the substrate to drive catalysis (*60*), metalloregulators such as NikR must be able to direct some of the free energy of metal binding toward a protein conformational change that moderates the DNA-binding activity. This redirection of binding energy toward a protein conformational change is also a key element in metalloproteins with a purely structural metal cofactor (*61*). NikR is better protected from denaturation by nickel than any other metal, and only nickel stabilizes both the metal-binding and the DNA-binding domains, suggesting that this metal induces a unique conformational change. This hypothesis is supported by the requirement for nickel in the high-affinity binding site in the metal-selective DNA-binding activity (*47*) as well as by protease digestion analysis of NikR bound to the different transition metals (A. Dias, D. Zamble, unpublished data). How this metal-selective effect of nickel is achieved is not clear. The fact that other metals can bind with similar or higher affinities but that the resulting proteins are easier to unfold suggests that these metals may destabilize the protein into a less active conformation, a general mechanism of functional specificity employed by metalloproteins (*62*).

Thus, unlike many other metalloregulators (*5*, *20*, *21*), the functional metal selectivity of NikR is not governed by metal-binding affinities. Instead, nickel binding is harnessed by NikR to produce a metal-selective allosteric effect. A similar situation was observed for the *Mycobacterium tuberculosis* NmtR transcriptional repressor that binds zinc more tightly then nickel or cobalt, but has a DNA-binding response only to nickel or cobalt (*10*). A recent spectroscopic study revealed that NmtR binds zinc in a four-coordinate site and nickel or cobalt in a five- or six-coordinate site, suggesting that its functional activity is linked to the coordination geometry induced by the metals in a flexible binding site. It is possible that the square-planar geometry of the nickel-binding site in NikR induces a metal-specific protein conformational change. However, the facts that other metals such as Cu(II) probably also bind in the same geometry and that the metal-binding site changes in the presence of DNA (*19*) suggest that the mechanism is more complex. Further studies will be needed to elucidate the detailed allosteric mechanism of this nickel-responsive metalloregulator.

ACKNOWLEDGMENT

We thank Prof. P. Chivers for the generous donation of the pNIK103 plasmid and for advice. We are also grateful to Prof. C. Drennan for helpful discussions as well as Profs. A. Woolley and R. Kluger and members of the Zamble laboratory.

REFERENCES

1. Watt, R. K., and Ludden, P. W. (1999) Nickel-binding proteins, *Cell. Mol. Life Sci. 56*, 604−625.
2. Maroney, M. J. (1999) Structure/function relationships in nickel biochemistry, *Curr. Opin. Chem. Biol. 3*, 188−199.
3. Barceloux, D. G. (1999) Nickel, *Clin. Toxicol. 37*, 239−258.
4. Costa, M., Yan, Y., Zhao, D., and Salnikow, K. (2003) Molecular mechanisms of nickel carcinogenesis: gene silencing by nickel delivery to the nucleus and gene activation/inactivation by nickel-induced cell signaling, *J. Environ. Monit. 5*, 222−223.
5. Busenlehner, L. S., Pennella, M. A., and Giedroc, D. P. (2003) The SmtB/ArsR family of metalloregulatory transcriptional repressors: structural insights into prokaryotic metal resistance, *FEMS Microbiol. Rev. 27*, 131−143.
6. Finney, L. A., and O'Halloran, T. V. (2003) Transition metal speciation in the cell: insights from the chemistry of metal ion receptors, *Science 300*, 931−936.
7. Eitinger, T., and Mandrand-Berthelot, M.-A. (2000) Nickel transport systems in microorganisms, *Arch. Microbiol. 173*, 1−9.
8. Mulrooney, S. B., and Hausinger, R. P. (2003) Nickel uptake and utilization by microorganisms, *FEMS Microbiol. Rev. 27*, 239−261.
9. Kim, J.-S., Kang, S.-O., and Lee, J. K. (2003) The protein complex composed of nickel-binding SrnQ and DNA-binding motif-bearing SrnR of *Streptomyces griseus* represses sodF transcription in the presence of nickel, *J. Biol. Chem. 278*, 18455−18463.
10. Cavet, J. S., Meng, W., Pennella, M. A., Appelhoff, R. J., Giedroc, D. P., and Robinson, N. J. (2002) A nickel-cobalt-sensing ArsR-SmtB family repressor, *J. Biol. Chem. 277*, 38441−38448.
11. López-Maury, L., García-Domínguez, M., Florencio, F. J., and Reyes, J. C. (2002) A two-component signal transduction system involved in nickel sensing in the cyanobacterium *Synechocystis* sp. PCC 6803, *Mol. Microbiol. 43*, 247−256.
12. De Pina, K., Desjardin, V., Mandrand-Berthelot, M.-A., Giordano, G., and Wu, L.-F. (1999) Isolation and characterization of the *nikR* gene encoding a nickel-responsive regulator in *Escherichia coli*, *J. Bacteriol. 181*, 670−674.
13. Chivers, P. T., and Sauer, R. T. (2000) Regulation of high affinity nickel uptake in bacteria, *J. Biol. Chem. 275*, 19735−19741.
14. Contreras, M., Thiberge, J.-M., Mandrand-Berthelot, M.-A., and Labigne, A. (2003) Characterization of the roles of NikR, a nickel-responsive pleiotropic autoregulator of *Helicobacter pylori*, *Mol. Microbiol. 49*, 947−963.
15. Wu, L. F., and Mandrand-Berthelot, M. A. (1986) Genetic and physiological characterization of new *Escherichia coli* mutants impaired in hydrogenase activity, *Biochimie 68*, 167−179.
16. Chivers, P. T., and Sauer, R. T. (1999) NikR is a ribbon-helix-helix DNA-binding protein, *Protein Sci. 8*, 2494−2500.
17. Chivers, P. T., and Sauer, R. T. (2002) NikR repressor: high-affinity nickel binding to the C-terminal domain regulates binding to operator DNA, *Chem. Biol. 9*, 1141−1148.
18. Schreiter, E. R., Sintchak, M. D., Guo, Y., Chivers, P. T., Sauer, R. T., and Drennan, C. L. (2003) Crystal structure of the nickel-responsive transcription factor NikR, *Nat. Struct. Biol. 10*, 794−799.
19. Carrington, P. E., Chivers, P. T., Al-Mjeni, F., Sauer, R. T., and Maroney, M. J. (2003) Nickel coordination is regulated by the DNA-bound state of NikR, *Nat. Struct. Biol. 10*, 126−130.
20. Changela, A., Chen, K., Xue, Y., Holschen, J., Outten, C. E., O'Halloran, T. V., and Mondragón, A. (2003) Molecular basis of metal-ion selectivity and zeptomolar sensitivity by CueR, *Science 301*, 1383−1387.
21. Guedon, E., and Helmann, J. D. (2003) Origins of metal ion selectivity in the DtxR/MntR family of metalloregulators, *Mol. Microbiol. 48*, 495−506.
22. Pennella, M. A., Shokes, J. E., Cosper, N. J., Scott, R. A., and Giedroc, D. P. (2003) Structural elements of metal selectivity in metal sensor proteins, *Proc. Natl. Acad. Sci. U.S.A. 100*, 3713−3718.
23. Gill, S. C., and von Hippel, P. H. (1989) Calculation of protein extinction coefficients from amino acid sequence data, *Anal. Biochem. 182*, 319−326.
24. Martell, A. E., and Smith, R. M. (2003) *NIST Standard Reference Database 46*, Version 7.0, NIST, Gaithersburg, MD.
25. Perrin, D. D., and Dempsey, B. (1974) *Buffers for pH and metal ion control*, Chapman and Hall, London.
26. Fahrni, C. J., and O'Halloran, T. V. (1999) Aqueous coordination chemistry of quinolone-bases fluorescence probes for the biological chemistry of zinc, *J. Am. Chem. Soc. 121*, 11448−11458.
27. Kwan, C.-Y., and Putney, J. W. J. (1990) Uptake and intracellular sequestration of divalent cations in resting and methacholine-stimulated mouse lacrimal acinar cells, *J. Biol. Chem. 265*, 678−684.
28. Pace, C. N., and Scholtz, J. M. (1997) in *Protein structure: a practical approach* (Chreighton, T. E., Ed.) pp 299−321, Oxford University Press, London.
29. Tanford, C. (1970) Theoretical models for the mechanism of denaturation, *Adv. Protein Chem. 24*, 1−95.
30. Pace, C. N. (1986) Determination and analysis of urea and guanidine hydrochloride denaturation curves, *Methods Enzymol. 131*, 266−280.
31. Chen, X., Chu, M., and Giedroc, D. P. (2000) Spectroscopic characterization of Co(II)-, Ni(II)-, and Cd(II)-substituted wild-type and non-native retroviral-type zinc finger peptides, *J. Biol. Inorg. Chem. 5*, 93−101.
32. Lever, A. B. P. (1984) *Inorganic electronic spectroscopy*, 2nd ed., Elsevier Science, New York.
33. Amundsen, A. R., Whelan, J., and Bosnich, B. (1977) Biological analogues. On the nature of the binding sites of copper-containing proteins, *J. Am. Chem. Soc. 99*, 6730−6739.
34. Sugiura, Y. (1978) Newly synthesized sulfhydryl- and imidazole-containing tripeptides with a specific copper-binding site, *Inorg. Chem. 17*, 2176−2182.
35. Bharadwaj, P. K., Potenza, J. A., and Schugar, H. J. (1986) Characterization of [dimethyl N,N′-ethylenebis(L-cysteinato)-(2-)-S,S′]copper(II), Cu(SCH2CH(CO2CH3)NHCH2-)2, a stable Cu(II)-aliphatic dithiolate, *J. Am. Chem. Soc. 108*, 1351−1352.
36. Bertini, I., and Luchinat, C. (1984) High spin cobalt(II) as a probe for the investigation of metalloproteins, *Adv. Inorg. Biochem. 6*, 71−111.
37. Maret, W., and Vallee, B. L. (1993) Cobalt as probe and label of proteins, *Methods Enzymol. 226*, 52−71.
38. Lane, R. W., Ibers, J. A., Frankel, R. B., Papaefthymiou, G. C., and Holm, R. H. (1977) Synthetic analogues of the active sites of iron−sulfur proteins, *J. Am. Chem. Soc. 99*, 84−98.
39. May, S. W., and Kuo, J.-Y. (1978) Preparation and properties of cobalt(II) rubredoxin, *Biochemistry 17*, 3333−3338.
40. Hitomi, Y., Outten, C. E., and O'Halloran, T. V. (2001) Extreme zinc-binding thermodynamics of the metal sensor/regulator protein, ZntR, *J. Am. Chem. Soc. 123*, 8614−8615.
41. Tanaka, M., Funahashi, S., and Shirai, K. (1968) Kinetics of the ligand substitution reaction of the zinc(II)-4-(2-pyridylazo)-resorcinol complex with (ethylene glycol)bis(2-aminoethyl ether)-N,N,N′,N′-tetraacetic acid, *Inorg. Chem. 7*, 573−578.
42. Hunt, J. B., Neece, S. H., and Ginsburg, A. (1985) The use of 4-(2-pyridylazo)resorcinol in studies of zinc release from *Escherichia coli* aspartate transcarbamoylase, *Anal. Biochem. 146*, 150−157.
43. Walkup, G. K., and Imperiali, B. (1997) Fluorescent chemosensors for divalent zinc based on zinc finger domains. Enhanced oxidative stability, metal binding affinity, and structural and functional characterization, *J. Am. Chem. Soc. 119*, 3443−3450.
44. Vlčková, S., Jančář, L., Kubáň, V., and Havel, J. (1982) Spectrophotometric study of the complex equilibria of cadmium(II) ions with 4-(2-pyridylazo)resorcinol (PAR) using the squad-G program and the method of determining Cd(II) ions with PAR, *Collect. Czech. Chem. Commun. 47*, 1086−1099.
45. Henehan, C. J., Pountney, D. L., Zerbe, O., and Vašák, M. (1993) Identification of cysteine ligands in metalloproteins using optical and NMR spectroscopy: Cadmium-substituted rubredoxin as a model of $[Cd(CysS)4]^{2-}$ center, *Protein Sci. 2*, 1756−1764.
46. Busenlehner, L. S., Weng, T.-C., Penner-Hahn, J. E., and Giedroc, D. P. (2002) Elucidation of primary (α3N) and vestigial (α5) heavy metal-binding sites in *Staphylococcus aureus* pI258 CadC: evolutionary implications for metal ion selectivity of ArsR/SmtB metal sensor proteins, *J. Mol. Biol. 319*, 685−701.
47. Bloom, S. B., and Zamble, D. B. (2004) Metal-selective DNA-binding response of *Escherichia coli* NikR, *Biochemistry 43*, 10029−10038.
48. Grynkiewicz, G., Poenie, M., and Tsien, R. Y. (1985) A new generation of Ca^{2+} indicators with greatly improved fluorescence properties, *J. Biol. Chem. 260*, 3440−3450.
49. Wittung-Stafshede, P., Gomes, C. M., and Teixeira, M. (2000) Stability and folding of the ferredoxin from the hyperthermophilic archaeon *Acidianus ambivalens*, *J. Inorg. Biochem. 78*, 35−41.

50. Leckner, J., Bonander, N., Wittung-Stafshede, P., Malmström, B. G., and Karlsson, G. (1997) The effect of the metal ion on the folding energetics of azurin: a comparison of the native, zinc and apoprotein, *Biochim. Biophys. Acta 1342*, 19−27.
51. Robinson, C. R., Liu, Y., Thomson, J. A., Sturtevant, J. M., and Sligar, S. G. (1997) Energetics of heme binding to native and denatured states of cytochrome b562, *Biochemistry 36*, 16141−16146.
52. Apiyo, D., Guidry, J., and Wittung-Stafshede, P. (2000) No cofactor effect on equilibrium unfolding of *Desulfovibrio desulfuricans* flavodoxin, *Biochim. Biophys. Acta 1479*, 214−224.
53. Pozdnyakova, I., and Wittung-Stafshede, P. (2001) Copper binding before polypeptide folding speeds up formation of active (holo) *Pseudomonas aeruginosa* azurin, *Biochemistry 40*, 13728−13733.
54. Cotton, F. A., and Wilkinson, G. (1988) *Advanced Inorganic Chemistry*, 5th ed., Wiley-Interscience, New York.
55. Rulíšek, L., and Vondrášek, J. (1998) Coordination geometries of selected transition metal ions (Co^{2+}, Ni^{2+}, Cu^{2+}, Zn^{2+}, Cd^{2+} and Hg^{2+}) in metalloproteins, *J. Inorg. Biochem. 71*, 115−127.
56. Irving, H., and Williams, R. J. P. (1948) Order of stability of metal complexes, *Nature 162*, 746−747.
57. McCall, K. A., and Fierke, C. A. (2004) Probing determinants of the metal ion selectivity in carbonic anhydrase using mutagenesis, *Biochemistry 43*, 3979−3986.
58. Roder, H., and Colón, W. (1997) Kinetic role of early intermediates in protein folding, *Curr. Opin. Struct. Biol. 7*, 15−28.
59. Hargrove, M. S., and Olson, J. S. (1996) The stability of holomyoglobin is determined by heme affinity, *Biochemistry 35*, 11310−11318.
60. Jencks, W. P. (1975) in *Advances in Enzymology* (Meister, A., Ed.) pp 219−410, John Wiley & Sons, New York.
61. Barker, P. D. (2003) Designing redox metalloproteins from bottom-up and top-down perspectives, *Curr. Opin. Struct. Biol. 13*, 490−499.
62. Hellinga, H., W,. (1998) The construction of metal centers in proteins by rational design, *Folding Des. 3*, R1−R8.

BI049405C